

PARALLEL PATH MAGNET MOTOR: DEVELOPMENT
OF THE THEORETICAL MODEL AND ANALYSIS
OF EXPERIMENTAL RESULTSI. Dirba¹, J. Kleperis²¹Faculty of Physics, University of Latvia,²Institute of Solid State Physics, University of Latvia,

8 Kengaraga Str., Riga, LV-1063, LATVIA

e-mail: imants.dirba@gmail.com

Analytical and numerical modelling is performed for the linear actuator of a parallel path magnet motor. In the model based on finite-element analysis, the 3D problem is reduced to a 2D problem, which is sufficiently precise in a design aspect and allows modelling the principle of a parallel path motor. The paper also describes a relevant numerical model and gives comparison with experimental results. The numerical model includes all geometrical and physical characteristics of the motor components. The magnetic flux density and magnetic force are simulated using FEMM 4.2 software. An experimental model has also been developed and verified for the core of switchable magnetic flux linear actuator and motor. The results of experiments are compared with those of theoretical/analytical and numerical modelling.

Key words: *electric machines, switchable magnetic flux, parallel path magnetic technology (PPMT), analytical modelling, numerical modelling, finite-element method magnetics (FEMM).*

1. INTRODUCTION

Although electricity has been known for more than 2000 years and the electric motor – at least 200 years [1], their construction and materials used can still be improved. Nowadays, a great variety of electric motors exist, from which we set off direct current (DC) motors: brushed, brushless, pancake, stepper, etc.; and alternative current (AC) motors: shade-pole, induction, synchronous, universal, etc.. Figure 1 presents a detailed up-to-date classification of electric motors [2].

Among electric motors, the switched reluctance motor (SRM) – a synchronous machine which runs by reluctance torque – is becoming most popular. Because of the high efficiency in a wide operating range, absence of rotor windings, and maintenance-free operation, SRMs have some irrefutable advantages over other types of electric machines. The name “switched reluctance motor” was introduced by S.A. Nasar in 1969 [3], although the first recognizable reluctance machines were built more than 150 years ago (the most famous is Davidson’s traction drive for the electric locomotive, 1838) [4]. In 1995, Joe Flynn patented the parallel path magnetic technology (PPMT) [5] – an advanced magnetic force control technology applicable to motors, rotary and linear actuators, magnetic

latches, generators, etc.. The PPMT machines are based on permanent magnets controlled with a field coil in each parallel magnetic circuit. This revolutionary concept has been demonstrated in a wide variety of devices [6] but is neither completely understood nor modelled well enough mathematically.

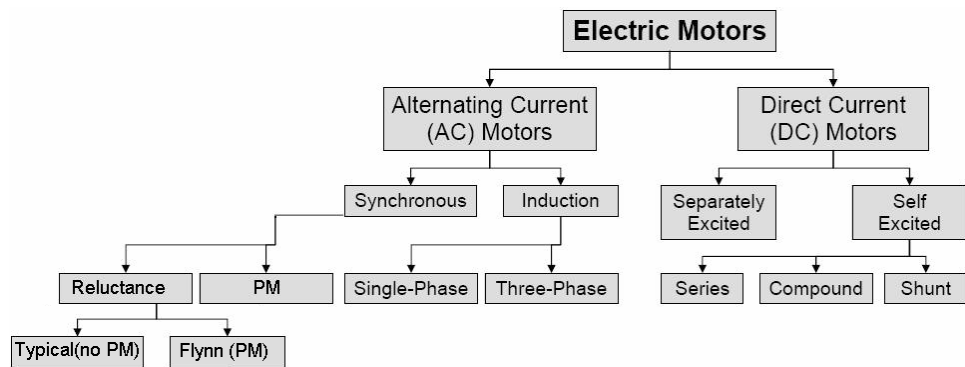


Fig. 1. Classification of the main types of electric motors [2].

The modelling of electrical machines is particularly important for studying their behaviour as well as in optimization tasks. Its methods can be categorized into the analytical modelling and the numerical modelling [7]. The analytical modelling has the advantage of rapidity, while its accuracy is not sufficient for optimization in a design process. At the same time, the numerical modelling is highly precise method but is time-consuming; nevertheless it is widely applied (see, e.g. [8, 9]). Calculation in the applications needs accuracy, whereas the time of simulation is of less importance. The numerical method is based on the discrimination of a calculation domain to finite elements and solution of Maxwell's equations for these elements [10]. In turn, the finite-element method magnetics (FEMM) can be categorized into three-dimensional (3D) and two-dimensional (2D) methods – the former being more time-consuming but possessing higher accuracy than the 2D modelling. Many researchers have demonstrated that the axial flux permanent magnet (AFPM) machines are intrinsically 3D ones; therefore, to accurately analyze the behaviour of these machines we should resort to the 3D-FEMM modelling, while reduction to a 2D problem is not desirable in the design process and sensitivity analysis [7–13].

This paper presents a theoretical development and analysis of the results of experiments and a 2D FEMM simulation of the working principle of PPMT linear actuators as well as the results obtained by calculation of the air-gap magnetic flux density and magnetic forces.

2. MODEL DESCRIPTION

The parallel path magnetic technology (PPMT) uses two or more permanent magnets placed in parallel. The basic magnetic circuit consists of a flux steering coil on each flux path as shown in Fig. 2. In the case there is no current in the coils, the magnetic circuit acts as if these coils are absent.

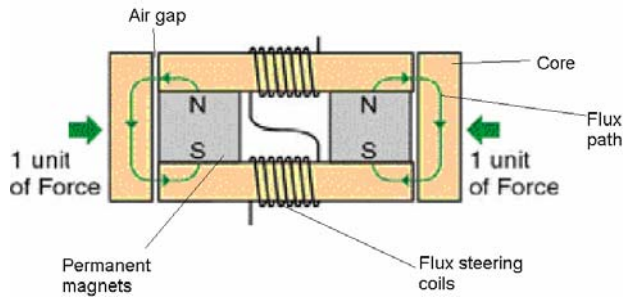


Fig. 2. Basic PPMT actuator (flux steering coils off) [6].

However, if current flows in the flux steering coils to produce a magnetic polarity as shown in Fig. 3, the magnetic flux produced by the coils couples with the permanent magnet's flux, and the result is four units of force (instead of two in Fig. 2 due to the squared force law of the combined permanent magnet flux) at one pole of the device. Once the flux has switched on, the actuation elements are moving to create an air gap on the zero-force side; the steering coils can thus be turned off, and the actuator or motor will remain in this new state – i.e. four units of permanent force with no power required. A momentary coil pulse of the opposite polarity will switch the actuator in the opposite direction (Fig. 3).

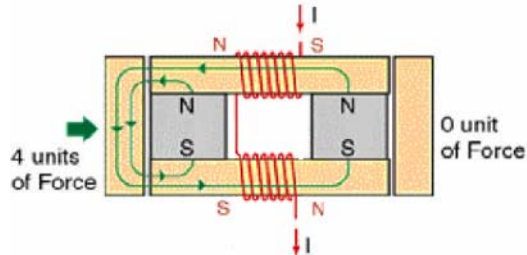


Fig. 3. Basic PPMT actuator steering coils for switching the whole magnetic flux to one actuator pole [6].

In the actuation of a PPMT device the steering coil only needs to have sufficient current to equalize the flux of one permanent magnet. Thus in such a device a given amount of magnetic flux can be controlled with only half the field coil power required by conventional devices.

3. MODEL CALCULATIONS

3.1. Simplified theoretical analysis of the PPMT device

3.1.1. Simplified analysis of a PPMT device in the case of no current in the coils

The boundary condition of the magnetic flux density component normal to the boundary between two environments (a and b in Fig. 4) with different permeability is:

$$B_{na} = B_{nb} . \quad (1)$$

The magnetic field in the air gap is approximately the same as in the conductor (since it is not dissipated). The line integral in Circulation Theorem of the

magnetic field can be decomposed into the magnetic field for each field conductor (Fig. 4):

$$\oint \frac{\vec{B}d\vec{l}}{l \mu} = \int \frac{\vec{B}d\vec{l}}{l_m \mu_m} + \int \frac{\vec{B}d\vec{l}}{l_2 \mu_{Fe}} + \int \frac{\vec{B}d\vec{l}}{l_g \mu_g} + \int \frac{\vec{B}d\vec{l}}{l_1 \mu_{Fe}} + \int \frac{\vec{B}d\vec{l}}{l_g \mu_g} + \int \frac{\vec{B}d\vec{l}}{l_2 \mu_{Fe}} = \mu_0 nI , \quad (2)$$

where: B – the magnetic field induction vector;
 l – the contour path length;
 μ – the permeability of the material;
 μ_0 – the magnetic constant (vacuum permeability);
 I – the current in the loop;
 N – the number of windings in the loop.

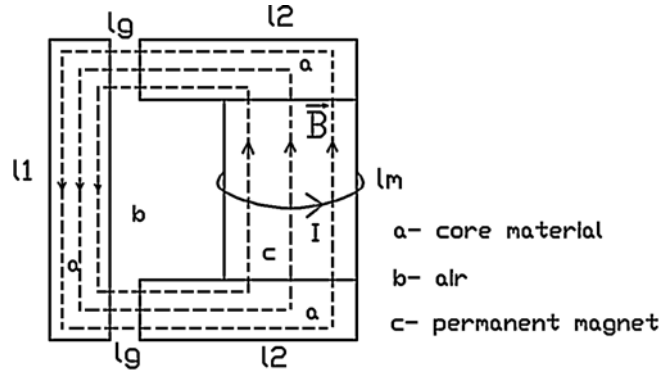


Fig. 4. Schematic of parallel path core for the case with flux steering coils off (Fig. 2).

From Eq. (2) according to Fig. 4 the following relationship is obtained:

$$\frac{\vec{B}}{\mu_m} l_m + \frac{\vec{B}}{\mu_{Fe}} l_2 + \frac{\vec{B}}{\mu_g} l_g + \frac{\vec{B}}{\mu_{Fe}} l_1 + \frac{\vec{B}}{\mu_g} l_g + \frac{\vec{B}}{\mu_{Fe}} l_2 = \mu_0 nI . \quad (3)$$

In turn, from Eq. (3) the following equation for the air-gap magnetic flux density is derived:

$$\Rightarrow \vec{B} = \frac{\mu_0 nI}{\frac{l_m}{\mu_m} + \frac{l_2}{\mu_{Fe}} + \frac{l_g}{\mu_g} + \frac{l_1}{\mu_{Fe}} + \frac{l_g}{\mu_g} + \frac{l_2}{\mu_{Fe}}} . \quad (4)$$

For identifying the term nI in Eq. (4), the permanent magnet is considered as material consisting of internal micro-currents [14]; therefore the current loops inside the material are opposite and compensate each other. Thus we can only deal with the current loop lying on the surface of material. The Biot–Savart law relates magnetic fields to the currents which are their sources (Fig. 5). Therefore, for the magnetic field induction in the centre of permanent magnet (if it is described with a current loop having radius vector r_0 lying on the surface) we have:

$$B = \frac{\mu_0 I}{2r_0} . \quad (5)$$

Knowing the residual flux density, magnetic permeability, magnetic flux and sizes of the permanent magnet, the current in the current loop lying on the surface can be calculated as

$$I = \frac{B \cdot 2 \cdot r_0}{\mu_0 \mu} = \frac{1.2 \cdot 2 \cdot 0.006}{1.05 \cdot 4\pi \cdot 10^{-7}} = 10913 \text{ A} . \quad (6)$$

Therefore, the air-gap magnetic flux density can be derived from Eq. (4):

$$\Rightarrow \vec{B} = \frac{\mu_0 n I}{\frac{l_m}{\mu_m} + \frac{l_2}{\mu_{Fe}} + \frac{l_g}{\mu_g} + \frac{l_1}{\mu_{Fe}} + \frac{l_g}{\mu_g} + \frac{l_2}{\mu_{Fe}}} = \frac{4\pi \cdot 10^{-7} \cdot 10913}{0.03} \approx 0.45 \text{ T} , \quad (7)$$

where: \vec{n} – the normal vector;

\vec{r}_0 – the radius vector;

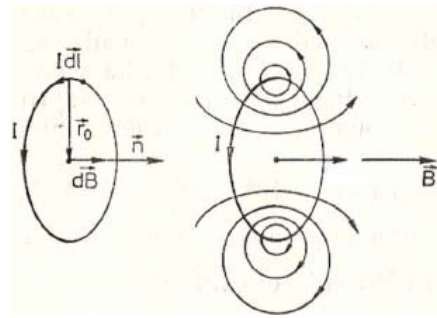


Fig. 5. Biot-Savart law ([15]).

The force is calculated from Maxwell's stress tensor:

$$T_{ik} = \varepsilon_0 E_i E_k + \frac{1}{\mu_0} B_i B_k - \frac{\delta_{ik}}{2} \left(\varepsilon_0 \vec{E}^2 + \frac{1}{\mu_0} \vec{B}^2 \right), \text{ N/m}^2. \quad (8)$$

As forces are produced only by magnetic field, Eq. (8) reduces to:

$$T_{ik} = \frac{1}{\mu_0} B_i B_k - \frac{\delta_{ik}}{2} \frac{1}{\mu_0} \vec{B}^2, \text{ N/m}^2. \quad (9)$$

From Fig. 6 it is seen that only the xx -component of Maxwell's stress tensor is left:

$$T_{xx} = \frac{1}{\mu_0} B_x B_x - \frac{1}{2} \frac{1}{\mu_0} \vec{B}^2 = \frac{1}{2} \frac{1}{\mu_0} B^2, \text{ N/m}^2. \quad (10)$$

The width and height of the rectangular core cross-section is 25 mm, therefore the force for both core sides will be:

$$\vec{F} = \oint_{\sigma} T_{ik} d\vec{S} = T_{xx} \Delta S = \frac{B^2}{2\mu_0} S = \frac{0.45^2}{2\mu_0} \cdot 0.025 \cdot 0.025 \cdot 2 = 100 \text{ N}. \quad (11)$$

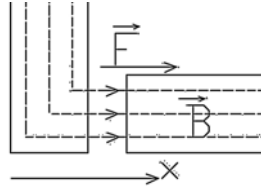


Fig. 6. Geometry of the calculated force.

3.1.2. Simplified analysis of PPMT device in the case with current in the coils

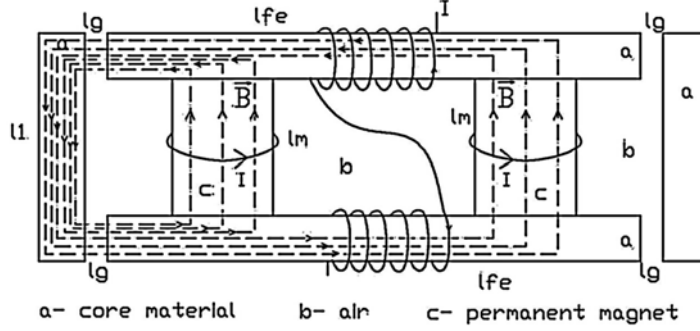


Fig. 7. Schematic of the parallel path core for the case of steering coils engaged (Fig. 3).

If we suppose that the core is not saturated, from the superposition principle the magnetic field induction in the air gap is found via summation of the value calculated by Eq. (7) and the values of magnetic field induction produced by the second magnet and by the current coils. Thus for the case shown in Fig. 7 we will have:

$$\bar{B}_{\Sigma} = 0.45 \text{ T} + \frac{\mu_0 \Sigma n I}{\frac{l_m}{\mu_m} + \frac{l_{fe}}{\mu_{Fe}} + \frac{l_g}{\mu_g} + \frac{l_1}{\mu_{Fe}} + \frac{l_g}{\mu_g} + \frac{l_{fe}}{\mu_{Fe}}} = 0.90 \text{ T}$$

and, therefore, the force is:

$$\vec{F} = \frac{B^2}{2\mu_0} S = \frac{0.90^2}{2\mu_0} \cdot 0.00125 = 402 \text{ N}.$$

If we suppose that the core is not saturated, from the superposition principle the magnetic field induction in the air gap is found via summation of the value calculated by Eq. (7) and the values of magnetic field induction produced by the second magnet and by the current coils. Thus for the case shown in Fig. 7 we will have:

$$\bar{B}_{\Sigma} = 0.45 \text{ T} + \frac{\mu_0 \Sigma n I}{\frac{l_m}{\mu_m} + \frac{l_{fe}}{\mu_{Fe}} + \frac{l_g}{\mu_g} + \frac{l_1}{\mu_{Fe}} + \frac{l_g}{\mu_g} + \frac{l_{fe}}{\mu_{Fe}}} = 0.90 \text{ T} \quad (12)$$

and, therefore, the force is:

$$\vec{F} = \frac{B^2}{2\mu_0} S = \frac{0.90^2}{2\mu_0} \cdot 0.00125 = 402 \text{ N}. \quad (13)$$

3.2. Numerical modelling of the PPMT device

This modelling is based on the finite element method magnetics (FEMM 4.2), which is an open source Windows finite element solver for the 2D and axisymmetric magnetic, electrostatic, heat flow and current flow problems with graphical pre- and post-processors. The FEMM is licensed under the terms of the Aladdin Free Public License (the author David Meeker, Ph.D). The Triangle mesh generator and the Lua scripting language, which are included in the distribution, each have their own licensing terms. In our case a 2D magnetic problem is considered, i.e. the magnetic field lines, vectors, air-gap flux density, and force are plotted in a xy -plane with the user-defined constant z -axis value). The simulations were made for a simplified scheme describing the operation of PPMT mechanism (Fig. 8). The core of the magnetic machine under consideration is made from four rectangle pieces of packed transformer steel sheets and permanent magnets (a and c, respectively, in Fig. 8). Current coils d are wound around two parallel core elements.

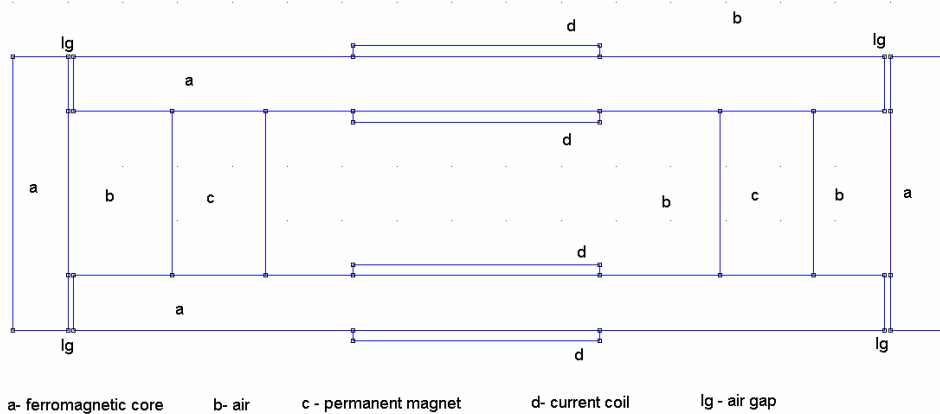


Fig. 8. Geometry of the simulated magnetic system.

The 2D FEMM model shown in Fig. 8 was built using a triangular 1mm-sized grid. Different ferromagnetic core materials (pure iron, electrical steel) were also analysed. It was assumed that air (with relative magnetic permeability equal to 1) fills the free space.

3.2.1. Numerical modelling of a PPMT device in the case without current in the coils

The output of numerical calculations for the geometry shown in Fig. 8 is displayed in Fig. 9, with magnetic field lines and vectors in the system formed by permanent magnets depicted for the no-current case.

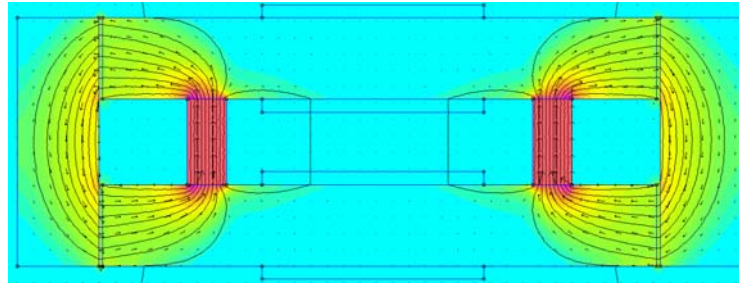


Fig. 9. Simulation for PPTM in the no-current case: the resultant magnetic field density, field lines and vectors.

The magnetic field density in the air-gap is shown in Fig. 10. As is seen, the magnetic field is not dissipated, so in the air-gap it is approximately the same as in the conductor (in compliance with the approximation made in Ch. 3.1).

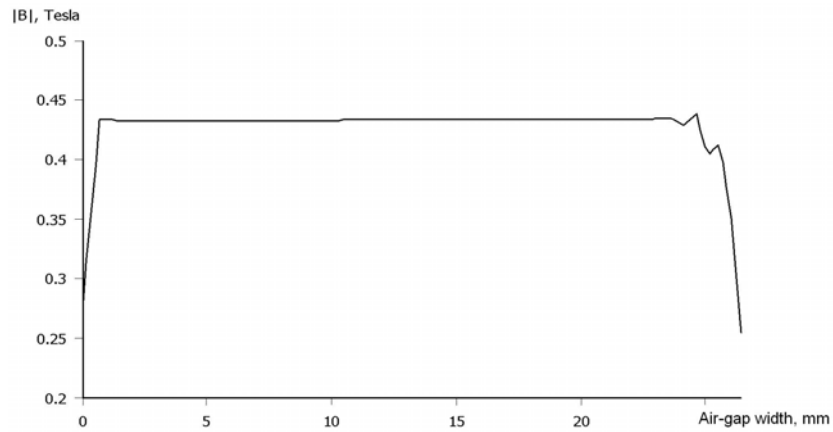


Fig. 10. Magnetic flux density in the air-gap of the simulated magnetic system.

The core-side magnetic attraction force was calculated by FEMM 4.2 using Maxwell's stress tensor, with the resultant value of 69 N.

3.2.2. Numerical modelling of a PPMT device in the case with current in the coils

Figure 11 shows the magnetic field lines and vectors for the system formed by permanent magnets in the case with steering coils (the output of numerical calculations for the geometry depicted in Fig. 3 is presented above).

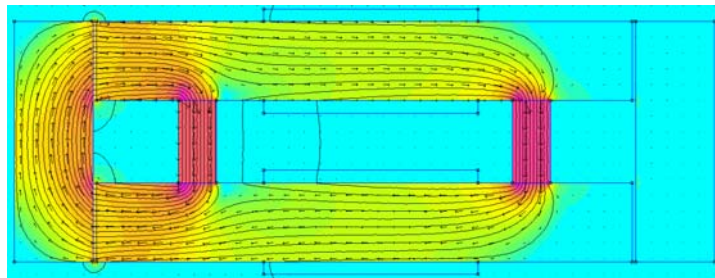


Fig. 11. Magnetic field density, field lines, and vectors in the case of current in the coils.

The magnetic flux produced by the current coils couples with the permanent magnet's flux and the result is a doubled magnetic flux density. The ferromagnetic core is almost saturated, therefore it is impossible to apply stronger (N52) NdFeB magnets. The core-side magnetic attraction force was again calculated using Maxwell's stress tensor, with the value of 360 N obtained.

4. COMPARISON OF SIMULATION AND EXPERIMENTAL RESULTS

The experimental setup was made in compliance with the geometry shown in Fig. 9. A Zwick/Roell BDO-FB005TN machine for testing materials (Fig. 12) with the maximum tension load of 5 kN was used to experimentally obtain the core-side magnetic attraction force.



Fig. 12. Experimental setup: a Zwick/Roell BDO-FB005TN testing machine with a test sample.

A PPTM device was mounted in the testing machine and the required critical force values were identified in a stretching process. The experimentally determined core-side magnetic attraction forces, together with analytical and numerical calculation results, are presented in Table 1.

Table 1

Comparison of the simulated and experimentally obtained results

Model	Core-side attraction force, N	
	Case Fig. 2	Case Fig. 3
Analytical	100	402
Numerical	96	360
Experimental	81	305

As is seen from Table 1, the obtained analytical, numerical and experimental results are comparable, therefore it could be inferred that the theoretical model and simulation methods proposed in this paper are applicable. The smaller value of force (81 N) in the experimental results is due to spacers – as the force value decreases almost four times compared with the case of Fig. 3, the linear size of these spacers increases; therefore, the air-gap flux density decreases, which leads to a reduced value of force. The second experimental value is smaller than the nume-

rical credible because of saturation effects in the core material (not taken into account in our simplified analytical model) and also the fringing effect of magnetic flux in the air-gap.

In this paper we illustrate the basic working principle of the PPMT ideology. Further research on the PPMT motor will be done with the first prototype (Figs. 13, 14) built according to the circuit sketched in work [6].

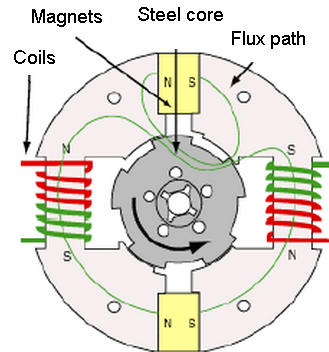


Fig. 13. Switchable PPMT motor – basic circuit arrangement [6].



Fig. 14. Switchable PPMT motor (the prototype).

5. CONCLUSIONS

A two-dimensional finite element model has been employed to analyze accurately the working principle of a switchable PPMT motor. The air-gap flux density and magnetic force values were calculated using the developed model, and it is shown that the simulation results are in a good agreement with the theoretically calculated (variation in the air-gap magnetic flux density values is only $\sim 4.4\%$) and experimentally measured values.

When current is flowing in the flux steering coils producing the magnetic polarity, the produced magnetic flux couples with the permanent magnet's flux, with the result being almost four units of force (instead of two due to the squared force law of the combined permanent magnet flux) at one pole of the device. In the actuation of PPMT device a steering coil only needs to have sufficient current to equalize the flux of one permanent magnet. Thus, in the PPMT devices a given amount of magnetic flux can be controlled with only half power in the coil as compared with conventional electric machines.

Acknowledgements

The authors acknowledge Gatis Arents for technical assistance. One of the authors (I.D.) acknowledges the European Social Fund for scholarship.

REFERENCES

1. Dale, P.R., & Stephen, F.W. (2010). *Rotating Electrical Machines and Power Systems* (2nd ed-n). Fairmont Press, Inc., 399.
2. Energy Efficiency Guide for Industry in Asia (2006). UNEP[©] <http://www.energyefficiencyasia.org/>.
3. Nasar, S.A. (1969). DC Structures Reluctance Motor. *IEE Proceedings*, 116, 1048-9.
4. Eberle, U., & von Helmolt, R. (2010). *Energy Environ. Sci.*, (3), 689–699.
5. Flynn, C.J. (1995). US Patent No 5455474.
6. Flynn, C.J., Talsoe, N.B., & Childress, J.J. (2006). Space Tech.& Applic.: 3rd Symp.New Frontiers & Future Concepts. *AIP Conf. Proceedings*, 813, 1205–1212.
7. Krishnan, R. (2001) *Electric Motor Drives: Modelling, Analysis, and Control*. Prentice Hall, 626.
8. Hameyer, K. (1999). Numerical Modelling and Design of Electrical Machines and Devices. *Book Series: Advances in Electrical and Electronic Engineering*, (1).
9. Vese, I.-C., Marignetti, F., & Radulescu. M.M. (2010). *IEEE Transactions on Industrial Electronics*, 57, 320 – 326.
10. Dolinar, D., De Weerd, R., Belmans, R., & Freeman, E.M. (1997). *IEEE Transactions on Energy Conversion*, 12, 133-142.
11. Hameyer, K., Henrotte, F., Sande, H.V., Deliège, G., & De Gerssem, H. (2002). *Proc. Int. Conf.*, Gramado: CBMag (Brasil), 13.
12. Niazi, P. (2005). *Thesis at Texas A&M University*, 153.
13. Sundaram, M., Navaneethan P., & Vasanthakumar, M. (2009). *ICGST-ACSE J.*, (9), 49–53.
14. Feynman, R.P. (1971). *The Feynman Lectures on Physics*, vol. II, Addison–Wesley, 592.
15. Platacis, J. (1974). *Elektrība*. Rīga: Zvaigzne, 503.

TEORĒTISKĀ MODEĻA IZSTRĀDE UN EKSPERIMENTĀLO REZULTĀTU ANALĪZE PĀRSLĒDZAMU PARALĒLU MAGNĒTISKO PLŪSMU ELEKTRISKAJAI MAŠĪNAI

I. Dirba, J. Kleperis

Kopsavilkums

Pirmo reizi veikta pārslēdzamas magnētiskās plūsmas elektriskās mašīnas matemātiskā modelēšana un iegūti rezultāti, kas apliecina šāda tipa elektriskās mašīnas darbības efektivitāti. Mūsdienās bieži optimāla dizaina modelēšana pastāvīgo magnētu (PM) motoriem tiek veikta, izmantojot galīgoelementu analīzes metodi. Konkrēti šajā darbā izmantotais modelis balstīts uz trīs dimensiju problēmas reducēšanu divu dimensiju problēmā, tādējādi ievērojami samazinot skaitliskajiem aprēķiniem nepieciešamo laiku un datora resursus. Tiek uzskatīts, ka apskatāmās problēmas ir simetriskas z plaknē, tādējādi trešās dimensijas neaplūkošana kļūdu

nerada. Šajā rakstā tiek apskatīts skaitliskais (galīgo elementu metode divās dimensijās) un tuvināts teorētiskais modelis pārslēdzamas magnētiskas plūsmas elektriskās mašīnas principa demonstrējumam. Darbā iegūtas magnētiskā lauka līniju, magnētiskā lauka indukcijas vektoru piesātinājuma indukcijas, magnētiskā spēka ainas, izmantojot skaitliskās modelēšanas paketi FEMM 4.2. Eksperimentālai pārbaudei izgatavots pārslēdzamas magnētiskas plūsmas elektriskās mašīnas principa demonstrējuma makets un iegūtie empīriskie rezultāti salīdzināti ar skaitliskā, tuvināta analītiskā risinājuma un modelēšanas rezultātiem.

12.05.2011